
FAST TRAINING OF LARGE KERNEL MODELS WITH DELAYED PROJECTIONS

Amirhesam Abedsoltan¹ Siyuan Ma² Parthe Pandit³ Mikhail Belkin¹

ABSTRACT

Classical kernel machines have historically faced significant challenges in scaling to large datasets and model sizes—a key ingredient that has driven the success of neural networks. In this paper, we present a new methodology for building kernel machines that can scale efficiently with both data size and model size. Our algorithm introduces delayed projections to Preconditioned Stochastic Gradient Descent (PSGD) allowing the training of much larger models than was previously feasible, pushing the practical limits of kernel-based learning. We validate our algorithm, EigenPro 4, across multiple datasets, demonstrating drastic training speed up over the existing methods while maintaining comparable or better classification accuracy.

1 INTRODUCTION

Kernel methods have strong theoretical foundations and broad applicability. They have also served as the foundation for understanding many significant phenomena in modern machine learning (Jacot et al., 2018; Belkin et al., 2018; 2019; Zhang et al., 2021). Despite these advantages, the scalability of kernel methods has remained a persistent challenge, particularly when applied to large datasets. Addressing this limitation is critical for expanding the utility of kernel-based techniques in modern machine learning applications.

A naive approach for training kernel machines is to directly solve the equivalent kernel matrix inversion problem. In general, the computational complexity of solving the kernel matrix inversion problem is $O(n^3)$, where n is the number of training samples. Thus, computational cost grows rapidly with the size of the dataset, making it computationally intractable for datasets with more than $\sim 10^5$ data points.

To address this challenge, various methods employing iterative algorithms and approximations have been proposed. Among these, Gradient Descent (GD)-based algorithms like Pegasos (Shalev-Shwartz et al., 2007) and EigenPro 1.0,2.0 (Ma and Belkin, 2017; 2019) have significantly reduced the computational complexity to $O(n^2)$. These methods, adaptable for stochastic settings, offer more efficient implementations. Nevertheless, the scalability of kernel machines remains constrained by the inherent linkage between the model size and the training set.

Furthermore, the Nyström methods have emerged as a favored approach for scaling kernel machines, with seminal works with (Williams and Seeger, 2000) paving the

way. Methods such as NYTRO (Camoriano et al., 2016), Falkon (Rudi et al., 2017) and ASkotch (Rathore et al., 2024) leverage the Nyström Approximation (NA) in combination with other strategies to enhance performance. NYTRO merges NA with gradient descent to improve condition number, ASkotch combines it with block coordinate descent, whereas Falkon combines it with the Conjugate Gradient method, facilitating the handling of large training sets. However, these strategies are limited by model size due to memory restrictions, exhibiting quadratic scaling in relation to the size of the model. For instance, scaling Falkon (Meanti et al., 2020) method to a model size of 512,000 necessitates over 1TB of RAM, surpassing the capacity of most high-end servers available today.

Other lines of work in the Gaussian Processes literature, e.g., (Titsias, 2009; Wilson and Nickisch, 2015; Gardner et al., 2018; Matthews et al., 2017), use so-called *inducing points* to control model complexity. However, these methods face similar scaling issues as they require quadratic memory in terms of the number of inducing points, thus preventing scaling to large models.

Recently, EigenPro 3.0 was introduced in (Abedsoltan et al., 2023). Unlike previous versions, EigenPro 3.0 distangle the model from the training set, similar to Falkon, but with the added advantage that its memory requirements scale linearly with the model size. This advancement makes it feasible to tackle kernel models of sizes previously deemed unattainable. However, its per iteration time complexity remains quadratic relative to the model size, significantly slowing its practical application.

In this paper, we build upon EigenPro 3.0 and introduce EigenPro 4.0*. This new algorithm retains the advantageous

¹UC San Diego ²Google ³IIT Bombay. Correspondence to: Amirhesam Abedsoltan <aabedsoltan@ucsd.edu>, Siyuan Ma <siyuan.ma9@gmail.com>, Parthe Pandit <pandit@iitb.ac.in>.

*<https://github.com/EigenPro/EigenPro/tree/main>

features of EigenPro 3.0, such as decoupling the model from the training set and linear scaling in memory complexity. Moreover, it significantly improves upon the time complexity, achieving amortized linear scaling per iteration with respect to model size. We empirically verify that the proposed algorithm converges in fewer epochs, without compromising generalization performance.

1.1 Main contribution

Our method for kernel machine problems achieves three key advantages: (1) linear amortized time complexity per iteration, (2) linear memory scaling with model size, (3) comparable or superior performance compare to existing methods while achieving up to 600× speedup in our experiments, and (4) an empirically significant reduction in the number of epochs required for convergence, particularly for larger models. Figure 1 demonstrates these benefits on CIFAR5M data set.

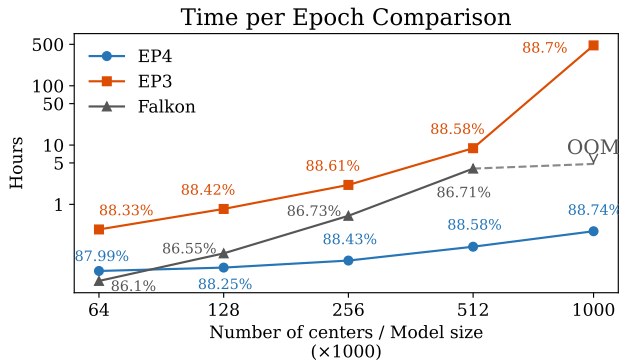


Figure 1: Per epoch time comparison between different solvers. Performance in terms of classification test accuracy (indicated as percentages) is annotated next to each data point, showing that EP4 maintains superior or comparable performance across all model sizes. The detail of the experiment can be found in Appendix C.

1.2 Organization of the Paper

The remainder of this paper is organized as follows. Section 2 provides the necessary background and preliminaries. In Section 3, we present a high-level overview of EigenPro 4 and introduce the key insights that enable its dramatic improvement in computational efficiency. In Section 4, we derive the complete algorithm and present our computational optimization techniques. Finally, Section 5 presents extensive experimental results across multiple datasets and model sizes.

2 NOTATION AND BACKGROUND

In what follows, functions are lowercase letters a , sets are uppercase letters A , vectors are lowercase bold letters \mathbf{a} ,

matrices are uppercase bold letters \mathbf{A} , operators are calligraphic letters \mathcal{A} , spaces and sub-spaces are boldface calligraphic letters \mathcal{A} .

General kernel models. Following EigenPro 3.0 (Abedsoltan et al., 2023) notations, given training data $(X, \mathbf{y}) = \{\mathbf{x}_i \in \mathbb{R}^d, y_i \in \mathbb{R}\}_{i=1}^n$, *General kernel models* are models of the form,

$$f(\mathbf{x}) = \sum_{i=1}^p \alpha_i K(\mathbf{x}, \mathbf{z}_i).$$

Here, $K : \mathbb{R}^d \times \mathbb{R}^d \rightarrow \mathbb{R}$ is a positive semi-definite symmetric kernel function and $Z = \{\mathbf{z}_i \in \mathbb{R}^d\}_{i=1}^p$ is the set of *centers*, which is not necessary the same as the training set. We will refer to p as the *model size*. We further define \mathcal{H} is the (unique) reproducing kernel Hilbert space (RKHS) corresponding to K .

Loss function. Our goal will be to find the solution to the following infinite-dimensional Mean Squared Error (MSE) problem for general kernel models,

$$\underset{f \in \mathcal{H}}{\text{minimize}} \quad L(f) = \sum_{i=1}^n (f(\mathbf{x}_i) - y_i)^2, \quad (1)$$

$$\text{subject to} \quad f \in \mathcal{Z} := \text{span}\left(\{K(\cdot, \mathbf{z}_j)\}_{j=1}^p\right). \quad (2)$$

Evaluations and kernel matrices. The vector of evaluations of a function f over a set $X = \{\mathbf{x}_i\}_{i=1}^n$ is denoted $f(X) := (f(\mathbf{x}_i)) \in \mathbb{R}^n$. For sets X and Z , with $|X| = n$ and $|Z| = p$, we denote the kernel matrix $K(X, Z) \in \mathbb{R}^{n \times p}$, while $K(Z, X) = K(X, Z)^\top$. Similarly, $K(\cdot, X) \in \mathcal{H}^n$ is a vector of functions, and we use $K(\cdot, X)\boldsymbol{\alpha} := \sum_{i=1}^n K(\cdot, \mathbf{x}_i)\alpha_i \in \mathcal{H}$, to denote their linear combination. Finally, for an operator \mathcal{A} , a function a , and a set $A = \{\mathbf{a}_i\}_{i=1}^k$, we denote the vector of evaluations of the output,

$$\mathcal{A}\{a\}(A) := (b(\mathbf{a}_i)) \in \mathbb{R}^k \quad \text{where} \quad b = \mathcal{A}(a). \quad (3)$$

Fréchet derivative. Given a function $J : \mathcal{H} \rightarrow \mathbb{R}$, the Fréchet derivative of J with respect to f is a linear functional, denoted $\nabla_f J$, such that for $h \in \mathcal{H}$

$$\lim_{\|h\|_{\mathcal{H}} \rightarrow 0} \frac{|J(f+h) - J(f) - \nabla_f J(h)|}{\|h\|_{\mathcal{H}}} = 0. \quad (4)$$

Since $\nabla_f J$ is a linear functional, it lies in the dual space \mathcal{H}^* . Since \mathcal{H} is a Hilbert space, it is self-dual, whereby $\mathcal{H}^* = \mathcal{H}$. If f is a general kernel model, and L is the square loss for a given dataset (X, \mathbf{y}) , i.e., $L(f) := \frac{1}{2} \sum_{i=1}^n (f(\mathbf{x}_i) - y_i)^2$ we can apply the chain rule, and using reproducing property

of \mathcal{H} , and the fact that $\nabla_f \langle f, g \rangle_{\mathcal{H}} = g$, we get, that the Fréchet derivative of L , at $f = f_0$ is,

$$\nabla_f L(f_0) = \sum_{i=1}^n (f_0(\mathbf{x}_i) - y_i) \nabla_f f(\mathbf{x}_i) \quad (5)$$

$$= K(\cdot, X)(f_0(X) - \mathbf{y}). \quad (6)$$

Hessian operator. The Hessian operator $\nabla_f^2 L : \mathcal{H} \rightarrow \mathcal{H}$ for the square loss is given by,

$$\mathcal{K} := \sum_{i=1}^n K(\cdot, \mathbf{x}_i) \otimes K(\cdot, \mathbf{x}_i), \quad (7)$$

$$\mathcal{K} \{f\}(\mathbf{z}) = \sum_{i=1}^n K(\mathbf{z}, \mathbf{x}_i) f(\mathbf{x}_i) = K(\mathbf{z}, X) f(X). \quad (8)$$

Operator \mathcal{K} has non-negative eigenvalues which we assume are ordered as $\lambda_1 \geq \lambda_2 \geq \dots \geq \lambda_n \geq 0$. Hence we have eigen-decompositions for this operator written as $\mathcal{K} = \sum_{i=1}^n \lambda_i \cdot \psi_i \otimes \psi_i$. Combining Equations 5 and 7, we can rewrite the Fréchet derivative of the loss function as following:

$$\nabla_f L(f_0)(z) = \mathcal{K} \{f_0(X) - \mathbf{y}\}(z) \quad (9)$$

Exact minimum norm solution. The closed-form minimum $\|\cdot\|_{\mathcal{H}}$ norm solution to the problem defined in equation (1) is given by:

$$\hat{f} := K(\cdot, Z) K^\dagger(Z, X) \mathbf{y}, \quad (10)$$

where $+$ is pseudoinverse or Moore–Penrose inverse. In the case of $X = Z$ it simplifies to $\hat{f} := K(\cdot, X) K^{-1}(X, X) \mathbf{y}$.

Gradient Descent (GD). If we apply GD on the optimization problem in 1, with learning rate η , in the \mathcal{H} functional space, the update is as following,

$$f_{t+1} = f_t - \eta \cdot \nabla_f L(f_t) \quad (11a)$$

$$= f_t - \eta K(\cdot, X) (f_t(X) - \mathbf{y}). \quad (11b)$$

The first point to note is that the derivative lies in $\mathcal{X} := \text{span} \left(\{K(\cdot, \mathbf{x}_j)\}_{j=1}^n \right)$ rather than in \mathcal{Z} . Therefore, when $X \neq Z$, SGD cannot be applied in this form. We will revisit this issue later. The second point is that in the case of $X = Z$, traditional *kernel regression* problem, the convergence of SGD depends on the condition number of \mathcal{K} . Simply put, this is the ratio of the largest to the smallest non-zero singular value of the Hessian operator defined in 7. It is known that for general kernel models this condition

number is usually ill conditioned and converges slow, see (Abedsoltan et al., 2024) for more details on this.

EigenPro. Prior work, EigenPro, by (Ma and Belkin, 2017), addresses the slow convergence of SGD by introducing a preconditioned stochastic gradient descent mechanism in Hilbert spaces. The update rule is the same as Equation 12 but with an additional preconditioner $\mathcal{P} : \mathcal{H} \rightarrow \mathcal{H}$ applied to the gradient,

$$f_{t+1} = f_t - \eta \cdot \mathcal{P} \nabla_f L(f_t). \quad (12)$$

In short, the role of the preconditioner \mathcal{P} is to suppress the top eigenvalues of the Hessian operator \mathcal{K} to improve the condition number. We next explicitly define \mathcal{P} .

Definition 1 (Top- q Eigensystem). Let $\lambda_1 > \lambda_2 > \dots > \lambda_n$ be the eigenvalues of a Hermitian matrix $\mathbf{A} \in \mathbb{R}^{n \times n}$, where for unit-norm \mathbf{e}_i , we have $\mathbf{A} \mathbf{e}_i = \lambda_i \mathbf{e}_i$. We define the tuple $(\Lambda_q, \mathbf{E}_q, \lambda_{q+1})$ as the top- q eigensystem, where:

$$\Lambda_q := \text{diag}(\lambda_1, \lambda_2, \dots, \lambda_q) \in \mathbb{R}^{q \times q}, \quad (13a)$$

$$\mathbf{E}_q := [\mathbf{e}_1, \mathbf{e}_2, \dots, \mathbf{e}_q] \in \mathbb{R}^{n \times q}. \quad (13b)$$

If $\mathbf{A} = K(X_s, X_s)$, we also define the following objects that is used in the iterations of EigenPro 4

$$\mathbf{D} := \Lambda^{-1} - \lambda_{q+1} \Lambda^{-2} \quad (14a)$$

$$\mathbf{F} := \mathbf{E} \sqrt{\mathbf{D}} \quad (14b)$$

Preconditioner. Using Definition 1, let $(\Lambda_q, \mathbf{E}_q, \lambda_{q+1})$ as the top- q eigensystem of $K(X, X)$, the preconditioner $\mathcal{P} : \mathcal{H} \rightarrow \mathcal{H}$ can be explicitly written as following,

$$\mathcal{P} := \mathcal{I} - \sum_{i=1}^q \left(1 - \frac{\lambda_{q+1}}{\lambda_i} \right) \psi_i \otimes \psi_i. \quad (15)$$

Nyström approximate preconditioner. EigenPro 2, introduced by (Ma and Belkin, 2019), implements a stochastic approximation for \mathcal{P} based on the Nyström extension, thereby reducing the time and memory complexity compared to EigenPro. The first step is to approximate the Hessian operator using the Nyström extension as follows,

$$\mathcal{K}^s := \sum_{k=1}^s K(\cdot, \mathbf{x}_{i_k}) \otimes K(\cdot, \mathbf{x}_{i_k}) \quad (16a)$$

$$= \sum_{i=1}^s \lambda_i^s \cdot \psi_i^s \otimes \psi_i^s. \quad (16b)$$

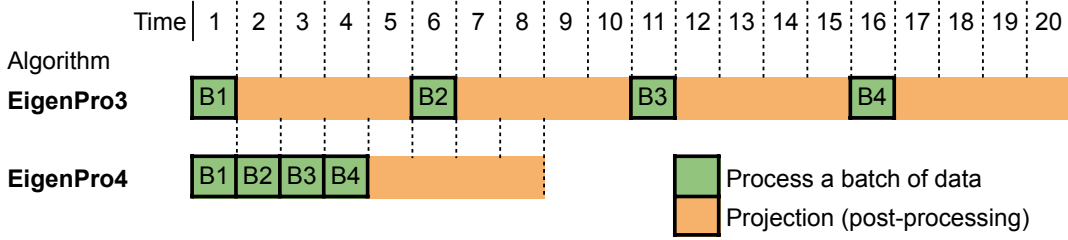


Figure 2: **Design of EigenPro4.** An illustration of how batches of data are processed by the two algorithms. EigenPro3 involves an expensive *projection* step when processing every batch of data. EigenPro4 waits for multiple batches to be processed before running the projection step for all of them together. This reduces the amortized cost for processing each batch.

This is a Nyström approximation of \mathcal{K} using s uniformly random samples from X , referred to as X_s , where $(\Lambda_q^s, \mathbf{E}_q^s, \lambda_{q+1}^s)$ represents the corresponding top- q eigen-system of $K(X_s, X_s)$. Using this approximation, we can define the approximated preconditioner as follows,

$$\mathcal{P}^s := \mathcal{I} - \sum_{i=1}^q \left(1 - \frac{\lambda_{q+1}^s}{\lambda_i^s}\right) \psi_i^s \otimes \psi_i^s \quad (17)$$

For more details on the performance of this preconditioner compared to the case of $s = n$, see [Abedsoltan et al. \(2024\)](#), who showed that choosing $s \gtrsim \log^4 n$ is sufficient.

Of particular importance is the action of this preconditioner on any function of the form $K(\cdot, A)\mathbf{u}$.

$$\mathcal{P}^s K(\cdot, A)\mathbf{u} = K(\cdot, A)\mathbf{u} - \sum_{i=1}^q \left(1 - \frac{\lambda_{q+1}^s}{\lambda_i^s}\right) \psi_i \psi_i(A)^\top \mathbf{u} \quad (18a)$$

$$= K(\cdot, A)\mathbf{u} - \sum_{i=1}^q \left(1 - \frac{\lambda_{q+1}^s}{\lambda_i^s}\right) \frac{K(\cdot, X_s) \mathbf{e}_i \mathbf{e}_i^\top K(X_s, A)}{\sqrt{\lambda_i} \sqrt{\lambda_i}} \mathbf{u} \quad (18b)$$

$$= K(\cdot, A)\mathbf{u} - K(\cdot, X_s) \mathbf{E} \mathbf{D} \mathbf{E}^\top K(X_s, A)\mathbf{u} \quad (18c)$$

$$= K(\cdot, A)\mathbf{u} - K(\cdot, X_s) \mathbf{F} \mathbf{F}^\top K(X_s, A)\mathbf{u} \quad (18d)$$

where recall the definitions of \mathbf{D} and \mathbf{F} in equation (14).

EigenPro 3. The primary limitation of EigenPro 2 was its inability to handle cases where $Z \neq X$, a necessary condition for disentangling the model and the training set. EigenPro 3 overcomes this limitation by recognizing that although the gradients in equation 5 may not lie within \mathcal{Z} , it is possible to project them back to \mathcal{Z} . Consequently, EigenPro 3 can be summarized as follows:

$$f_{t+1} = \text{proj}_{\mathcal{Z}} \left(f_t - \eta \mathcal{P}^s \{ \tilde{\nabla}_f L(f_t) \} \right), \quad (19)$$

where $\text{proj}_{\mathcal{Z}}(u) := \underset{f \in \mathcal{Z}}{\text{argmin}} \|u - f\|_{\mathcal{H}}^2$ for any $u \in \mathcal{H}$. As shown in ([Abedsoltan et al., 2023](#), Section 4.2), the exact projection is,

Algorithm	FLOPS		Memory
	setup	per sample	
EigenPro 4.0 (ours)	$O(1)$	$O(p)$	$O(p)$
EigenPro 3.0	$O(1)$	$O(p^2)$	$O(p)$
Falkon	$O(p^3)$	$O(p)$	$O(p^2)$

Table 1: **Algorithm complexity.** with respect to number of model centers p . Here we assumed only a constant number of epochs is needed for large scale experiments. Cost of kernel evaluations and number of classes are assumed to be $O(1)$.

$$\text{proj}_{\mathcal{Z}}(u) = K(\cdot, Z) K^{-1}(Z, Z) u(Z). \quad (20)$$

This projection can be interpreted as solving a kernel in \mathcal{Z} and can be approximated using EigenPro 2, as done in ([Abedsoltan et al., 2023](#)), with a time complexity that scales quadratically with model size. However, since this projection must be performed after each stochastic step, it becomes the most computationally expensive part of the EigenPro 3 algorithm.

3 EIGENPRO 4: ALGORITHM DESIGN

In this section, we provide a high-level overview and illustrations to highlight the key components of EigenPro 4 and how it significantly reduces training time.

3.1 Challenge to Scaling: High Overhead of Projection

The key development of EigenPro 3 over its contemporaries was that it could train models of this form in $O(p)$ memory. This was a huge improvement over the prior methods which required $O(p^2)$ memory ([Rudi et al., 2017](#); [Rathore et al., 2024](#)).

However, EigenPro 3 has a high cost $O(mp + p^2)$ per batch of data processed, as summarized in Table 1. This is espe-

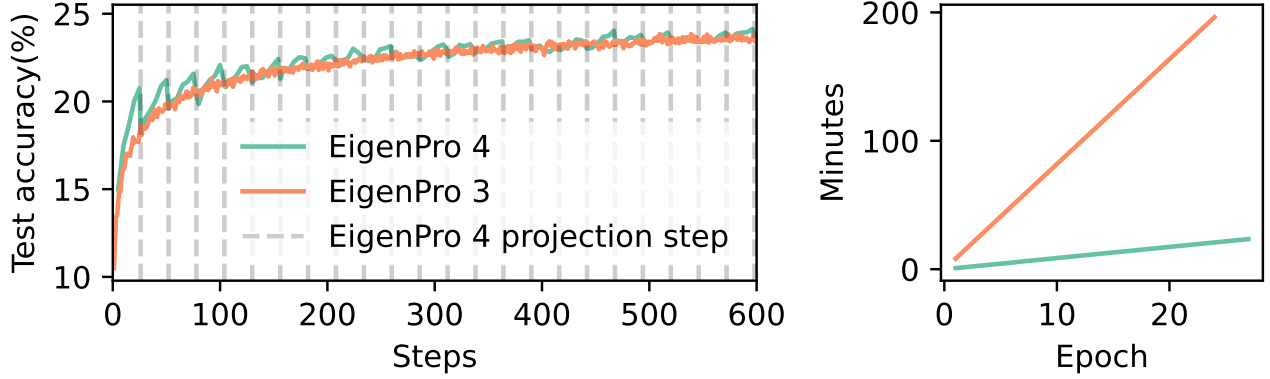


Figure 3: Performance and computational time comparison between EigenPro 4.0 ($T = 11$) and EigenPro 3.0 (equivalent to $T = 1$), highlighting the impact of the projection step on the performance of EigenPro 4.0. The detail of the experiment can be found in Appendix C.

cially expensive when $m \ll p$, i.e., when the batch size m is small compared to the model size p .

3.2 Main Idea: Delayed Projection

To address the computational complexity challenges, EP4 amortizes projection costs by delaying projections for T iterations. The value of T is a hyperparameter, with an effective selection method detailed in Section B. Figure 2 illustrates this delayed projection mechanism. ($T = 4$ in Figure 2)

In fact, EigenPro 3 is a special case of EigenPro 4 with parameter $T = 1$. However, we show in equation (34) that to minimize total time of training, the optimal value of T is in fact proportional to $\frac{p}{m}$. For this value of T , the cost of training per batch is $O(p)$.

Figure 3 shows how EigenPro 4 and EigenPro 3 perform over training iterations. EigenPro 4 accuracy improves between projections and drops after each projection step. While EigenPro 3 projects at every step, EigenPro 4 maintains comparable accuracy with fewer projections. The left panel of Figure 3 confirms that both methods reach similar final accuracy, while the right panel shows EigenPro 4 significant speed advantage. With continued training, EigenPro 4 accuracy drops from projections become progressively smaller.

4 EIGENPRO 4: ALGORITHM DEVELOPMENT AND OPTIMIZATION

In this section, we present the EigenPro 4 algorithm in three parts. First, we introduce the algorithm’s main components: the pre-projection and projection steps. Then, we detail each of these steps in the following two subsections. Finally, we describe a computational optimization that reduces the

runtime of EigenPro 4 by half.

4.1 Derivation of the EigenPro 4 Algorithm

As mentioned previously T is a crucial hyperparameter that determines the frequency of projection back to \mathcal{Z} after every T steps. Before the projection step T , at every step when a new batch (X_m, y_m) is fetched, it is added to a set defined as the “temporary centers” set, denoted by Z_{tmp} . Starting with an empty set, $Z_{\text{tmp}} = \emptyset$, we continuously add to Z_{tmp} with temporary centers until the step count reaches T .

Formally, the prediction function prior to the projection is no longer fixed and is now expanding. The model can be described as follows:

$$f(x) = \underbrace{\sum_{\mathbf{z} \in \mathcal{Z}} \alpha_{\mathbf{z}} K(\mathbf{x}, \mathbf{z})}_{\text{original model}} + \underbrace{\sum_{\mathbf{z} \in Z_{\text{tmp}}} \beta_{\mathbf{z}} K(\mathbf{x}, \mathbf{z})}_{\text{temporary model}} \quad (21)$$

where $\alpha_{\mathbf{z}}$ refers to the weights corresponding to the original model center \mathbf{z} and $\beta_{\mathbf{z}}$ refers to the weights corresponding to the temporary model center. We refer to the combination of original model and temporary model as auxiliary model. The full EigenPro 4 algorithm has been illustrated in Figure 4 and mathematically can be summarized as following,

$$f_t = \begin{cases} \text{proj}_{\mathcal{Z}} \left(f_{t-1} - \eta \mathcal{P}^s \{ \tilde{\nabla}_f L(f_{t-1}) \} \right), & t \equiv 0 \pmod{T}, \\ f_{t-1} - \eta \mathcal{P}^s \{ \tilde{\nabla}_f L(f_t) \}, & \text{otherwise.} \end{cases} \quad (22)$$

where $\tilde{\nabla} L$ is a stochastic gradient of the loss function computed over a mini-batch of data, and \mathcal{P}^s is a preconditioner.

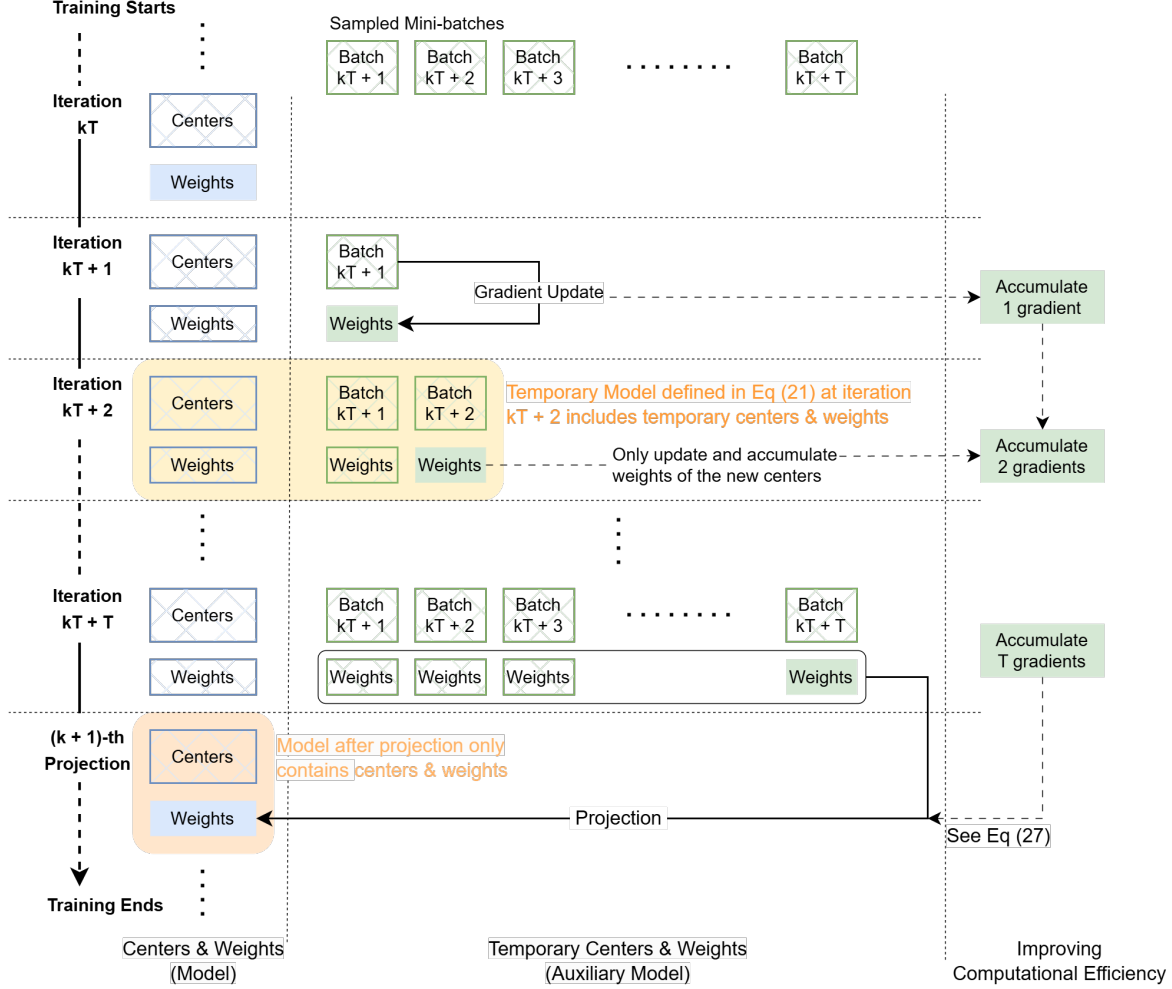


Figure 4: **Overview of iteration scheme for EigenPro4.** The figure illustrates how the model updates are performed over multiple iterations in EigenPro4. Weights are updated using batches, and gradients are accumulated iteratively until a projection step is executed. Temporary centers and weights are maintained during auxiliary iterations, which are merged through projection after a certain number of batches. This approach reduces the computational cost by accumulating gradients before performing the projection, leading to more efficient batch processing.

4.2 Pre-projection Steps

Based on Equation (22), suppose $(X_1, y_1), \dots, (X_T, y_T)$ are the minibatches of size m , and the initial model is $f_0 = K(\cdot, Z)\alpha$. After $t < T$ step, the following holds,

$$\begin{aligned} f_t &= f_{t-1} - \eta \mathcal{P}^s K(\cdot, X_t)(f_{t-1}(X_t) - y_t) \\ &= f_0 - \sum_{i=1}^t \mathcal{P}^s K(\cdot, X_i)(f_{i-1}(X_i) - y_i) \end{aligned}$$

Replacing \mathcal{P}^s with equation (16), $f_0 = K(\cdot, Z)\alpha$ and letting $(\Lambda_q, \mathbf{E}_q, \lambda_{q+1})$ be the top- q eigensystem of

$K(X_s, X_s)$, we can simplify the update above as following,

$$\begin{aligned} f_t &= K(\cdot, Z)\alpha_t \\ &\quad - \eta \sum_{i=1}^t \left(K(\cdot, X_i) \right. \\ &\quad \left. - K(\cdot, X_s) \mathbf{F} \mathbf{F}^\top K(X_s, X_i) \right) (f_{i-1}(X_i) - y_i) \\ &= K(\cdot, Z)\alpha - \sum_{i=1}^t K(\cdot, X_i) (\eta (f_{i-1}(X_i) - y_i)) \\ &\quad + K(\cdot, X_s) \sum_{i=1}^t \eta \mathbf{F} \mathbf{F}^\top K(X_s, X_i) (f_{i-1}(X_i) - y_i) \end{aligned} \tag{23}$$

where, $\mathbf{D} := \Lambda_q^{-1} (\mathbf{I}_q - \lambda_{q+1} \Lambda_q^{-1})$. This update rule implies that after t steps, the weights corresponding to the original centers Z remain unchanged to α , the weights for the temporary centers X_i are set once to $\eta(f_{i-1}(X_i) - y_i)$ after they are added, and do not change thereafter, and finally, the weights associated with the Nyström samples X_s are updated after each batch via an additive update. This is how we update the weights before projection at step T .

4.3 Projection Step: Update for $t = T$

Once, we reach step T we need to project f_T into \mathcal{Z} , or formally

$$f_T = \text{proj}_{\mathcal{Z}} \left(f_{T-1} - \eta \mathcal{P}^s \{ \tilde{\nabla}_f L(f_{T-1}) \} \right), \quad (24)$$

Applying Proposition 2 from [Abedsoltan et al. \(2023\)](#), the solution to this projection problem is as follows,

$$f_T = K(\cdot, Z) K^{-1}(Z, Z) f_{T-1}(Z) \quad (25)$$

Here, we define \mathbf{h} as the *accumulated gradient*.

The final EigenPro4 can be found in Algorithm 1. Note that we follow the same *inexact projection* scheme used in ([Abedsoltan et al., 2023](#)) to approximate the exact projection described in equation 25.

The benefit of this approximation is that we don't need to solve the problem exactly in \mathcal{X} , nor do we need to project back to \mathcal{Z} after each iteration. This approach offers the best of both worlds. In the next section, we demonstrate the effectiveness of this approach compared to prior state-of-the-art methods.

4.4 Improving Computational Efficiency

Upon careful examination of the derivations in equation 23, we observe that $f_{T-1}(Z)$ have already been computed previously. This allows us to efficiently reuse $f_{T-1}(Z)$ as follows,

$$\begin{aligned} f_{T-1}(Z) &= K(Z, Z) \alpha - \sum_{i=1}^{T-1} K(Z, X_i) (\eta(f_{i-1}(X_i) - y_i)) \\ &\quad + \sum_{i=1}^{T-1} K(Z, X_s) (\eta \mathbf{F} \mathbf{F}^\top K(X_s, X_i) (f_{i-1}(X_i) - y_i)) \\ &= K(Z, Z) \alpha - \sum_{i=1}^{T-1} K(Z, X_i) (\eta(f_{i-1}(X_i) - y_i)) \\ &\quad + \sum_{i=1}^{T-1} \eta (\mathbf{M} \mathbf{F}^\top K(X_s, X_i) (f_{i-1}(X_i) - y_i)) \end{aligned} \quad (26)$$

where $\mathbf{M} = K(Z, X_s) \mathbf{F}$. plugging this in equation 25 we obtain,

Algorithm 1 EigenPro 4

Require: Data (X, \mathbf{y}) , centers Z , batch size m , Nyström size s , preconditioner level q , projection period T

- 1: Fetch subsample $X_s \subseteq X$ of size s , corresponding weights $\alpha_s = 0$
- 2: $(\Lambda, \mathbf{E}, \lambda_{q+1}) \leftarrow$ top- q eigensystem of $K(X_s, X_s)$
- 3: $\mathbf{D} = (\Lambda^{-1} - \lambda_{q+1} \Lambda^{-2}) \in \mathbb{R}^{q \times q}$
- 4: $\mathbf{F} = \mathbf{E} \sqrt{\mathbf{D}} \in \mathbb{R}^{s \times q}$
- 5: $\mathbf{M} = K(Z, X_s) \mathbf{F} \in \mathbb{R}^{p \times q}$
- 6: $Z_{\text{tmp}} = \emptyset, \alpha_{\text{tmp}} = \emptyset, \alpha_s = \mathbf{0}_s, \mathbf{h} = \mathbf{0}_p$
- 7: **while** Stopping criterion is not reached **do**
- 8: **for** $t = \{1, 2, \dots, T\}$ **do**
- 9: Fetch minibatch (X_m, \mathbf{y}_m)
- 10: $\mathbf{g}_m \leftarrow K(X_m, Z) \alpha - \mathbf{y}_m$
- 11: $\mathbf{g}_m \leftarrow \mathbf{g}_m + K(X_m, Z_{\text{tmp}}) \alpha_{\text{tmp}}$
- 12: $\mathbf{g}_m \leftarrow \mathbf{g}_m + K(X_m, X_s) \alpha_s$
- 13: $Z_{\text{tmp}}.append(X_m)$
- 14: $\alpha_{\text{tmp}}.append(-\eta \cdot \mathbf{g}_m)$
- 15: $\alpha_s = \alpha_s + \eta \cdot \mathbf{F} \mathbf{F}^\top K(X_s, X_m) \mathbf{g}_m$
- 16: $\mathbf{h} \leftarrow \mathbf{h} - \eta \cdot K(Z, X_m) \mathbf{g}_m$
- 17: $\mathbf{h} \leftarrow \mathbf{h} + \eta \cdot \mathbf{M} \mathbf{F}^\top K(X_s, X_m) \mathbf{g}_m$
- 18: **end for**
- 19: $\theta \leftarrow \text{proj}_{\mathcal{Z}}(\mathbf{h})$
- 20: $\alpha \leftarrow \alpha - \frac{\eta}{m} \theta$
- 21: $Z_{\text{tmp}} \leftarrow \emptyset, \alpha_{\text{tmp}} \leftarrow \emptyset, \alpha_s \leftarrow \mathbf{0}_s, \mathbf{h} \leftarrow \mathbf{0}_p$
- 22: **end while**

$$f_T(Z) = K(\cdot, Z) (\alpha - K^{-1}(Z, Z) \mathbf{h}),$$

$$\begin{aligned} \mathbf{h} := & -\eta \left(\sum_{i=1}^{T-1} K(Z, X_i) ((f_{i-1}(X_i) - y_i)) \right. \\ & \left. + \sum_{i=1}^{T-1} (\mathbf{M} \mathbf{E}_q^\top K(X_s, X_i) (f_{i-1}(X_i) - y_i)) \right) \end{aligned} \quad (27)$$

4.5 Benefits of Approximate Preconditioning

Note that the preconditioner \mathcal{P}^s allows to drastically improve the speed of the iterations. But at the same time, the Nyström approximation also enables the algorithm to become tractable. Due to this approximate preconditioner, we only need to maintain s temporary centers in the auxiliary model, whereas the exact preconditioner ($s = n$) makes the algorithm intractable. Theoretically we only require $s = O(\log^4 n)$ as shown in ([Abedsoltan et al., 2024](#)).

5 NUMERICAL EXPERIMENTS

In this section, we demonstrate that our approach achieves orders of magnitude speedup over the state-of-the-art kernel methods while providing comparable or better generalization performance. We compare the performance of several kernel methods using the following data sets (1) CIFAR5M,

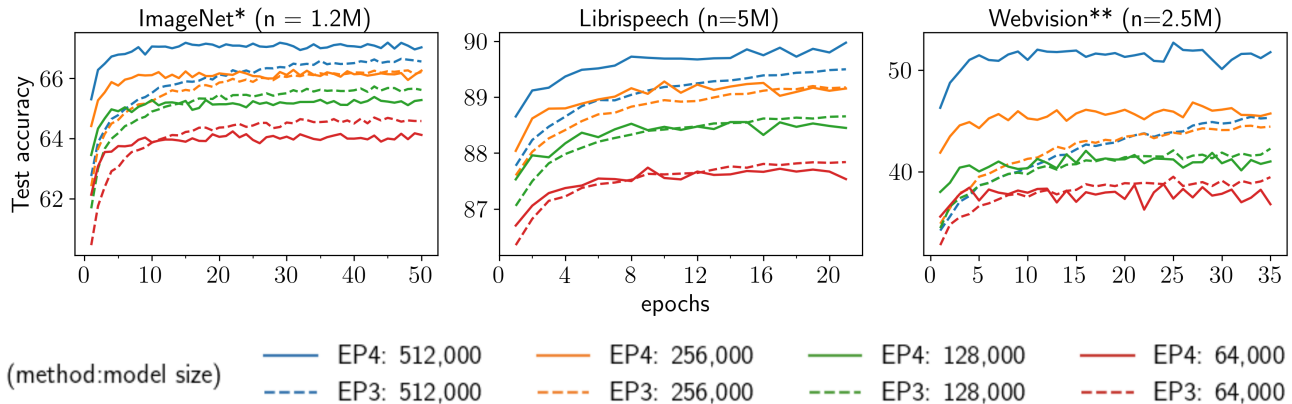


Figure 5: Multi-epoch performance and convergence comparison for EigenPro 3 and EigenPro 4. The detail of the experiment can be found in Appendix C.

CIFAR5M* (Nakkiran et al., 2021), (3) ImageNet*, (Deng et al., 2009), (4) Webvision**, (Li et al., 2017), and (8) Librispeech, (Panayotov et al., 2015). Details about datasets can be found in Appendix C. While our method is compatible with any kernel function, we opted for the Laplace kernel in our experiments due to its straightforward implementation and strong empirical performance. For handling multi-class classification, we decompose the problem into separate binary regression tasks, where each class is predicted using targets in $\{0, 1\}$. The final classification is determined by selecting the class with the maximum predicted value among all binary predictions. We run the experiments on a platform with one A100 GPU, one V100 GPU, and one Intel(R) Xeon(R) Gold 6248 CPU.

Substantial Reduction in Per-Epoch Training Time.

EigenPro 4 has substantially reduced the per-epoch training time, making it the most efficient kernel method on modern machine learning hardware. In contrast to performing projection every mini-batch iteration as in EigenPro 3, EigenPro 4 schedules one projection every few iterations such that its amortized cost is comparable to that of the standard iterations. This results in an ideal per-sample complexity $O(p)$, a remarkable improvement over the $O(p^2)$ complexity from EigenPro 3.

In Table 2, we evaluate the performance and computational timing for a single epoch of our proposed model against established kernel regression methods. As noted earlier, Falkon exhibits limitations due to its quadratic memory complexity. For the CIFAR5M* dataset, training with a model size of 512,000 required 1.3TB of RAM, while scaling to 1M model size necessitated over 5TB. Resource constraints limited our Falkon benchmarks to model sizes of

* feature extraction using MobileNetV2

** feature extraction using ResNet-18

128,000 and 64,000 for the remaining datasets. While EigenPro 3 addresses these memory constraints, it demonstrates significant computational overhead, particularly evident in the Librispeech dataset where our method, EigenPro 4, achieves a $411\times$ speedup. Notably, EigenPro 4 maintains comparable or superior performance across all evaluated datasets relative to both baseline methods.

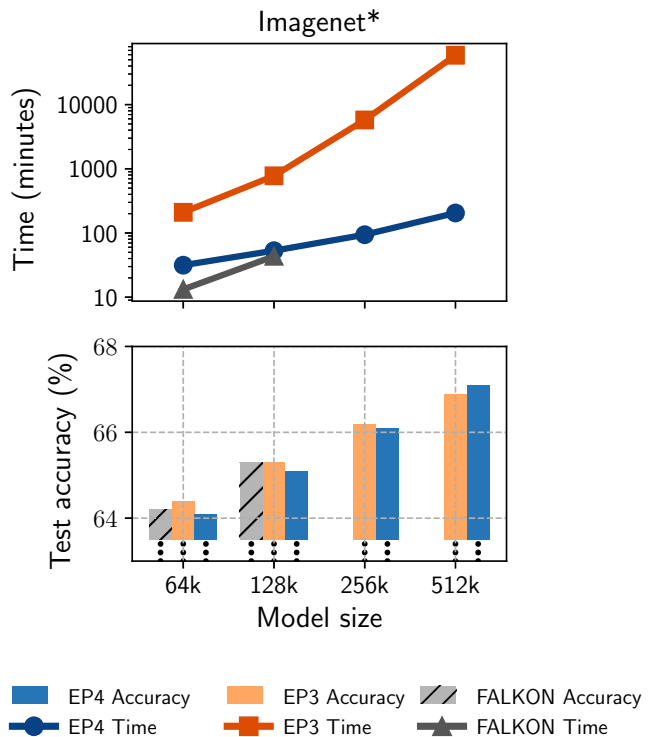


Figure 6: Time and performance comparison for Falkon, EigenPro 3 and EigenPro 4 for Imagenet data set. Details of the experiments can be found in Appendix C.

Fast training of large kernel models

Model size	Method	CIFAR5M*($n = 5M$)	CIFAR5M ($n = 6M$)	Librispeech ($n = 10M$)	Webvision ($n = 5.2M$)
p = 64K	EigenPro 4	5m (4.6x, 88%)	3m (15x, 69%)	16m (9.1x, 86.8%)	2m (45.5x, 24.3%)
	EigenPro 3	23m (1x, 88.3%)	45m (1x, 68.8%)	145m (1x, 85.4%)	91m (1x, 24%)
	Falkon	3m (7.67x, 86.1%)	5m (9x, 57.7%)	9m (16.11x, 81.0%)	4m (22.75x, 21.7%)
p = 128K	EigenPro 4	5m (10x, 88.25%)	4m (26.25x, 70.9%)	19m (17.95x, 87.8%)	4m (49.75x, 24.9%)
	EigenPro 3	50m (1x, 88.42%)	105m (1x, 70.3%)	341m (1x, 84.75%)	199m (1x, 24.5%)
	Falkon	9m (5.56x, 86.55%)	11m (9.55x, 59.4%)	21m (16.24x, 82.30%)	13m (15.31x, 22.4%)
p = 256K	EigenPro 4	7m (18.3x, 88.61%)	6m (130.8x, 71.8%)	24m (120x, 88.33%)	5m (106.2x, 26%)
	EigenPro 3	128m (1x, 88.61%)	785m (1x, 70.53%)	≈ 2 days (1x)	531m (1x, 25.52%)
	Falkon	38m (3.37x, 86.73%)	OOM	OOM	OOM
p = 512K	EigenPro 4	12m (44.25x, 88.58%)	10m (> 288x, 72.9%)	36m (> 200x, 88.89%)	11m (240x, 27.3%)
	EigenPro 3	531m (1x, 88.56%)	> 2 days (1x)	> 5 days (1x)	2 days (1x)
	Falkon	240m (2.21x, 86.71%)	OOM	OOM	OOM
p = 1M	EigenPro 4	21m (> 274x, 88.7%)	17m (> 508x, 73.8%)	70m (> 411x, 89.5%)	21m (> 686x, 29.3%)
	EigenPro 3	> 4 days (1x)	> 6 days (1x)	>20 days (1x)	> 10 days (1x)
	Falkon	OOM	OOM	OOM	OOM

Table 2: Comparison of EigenPro 4, EigenPro 3, and Falkon across different model sizes and datasets after 1 epoch. The values in parentheses represent the speedup in time over EigenPro 3 and the resulting accuracy. Details of the experiments can be found in Appendix C.

Linear Scaling with Model Size. The total training time and memory usage of EigenPro 4 scales linearly with the model size. In comparison, the time required for a single EigenPro 3 iteration grows quadratically with the model size, while the preprocessing time for Falkon grows cubically. Furthermore, the memory demand of Falkon increases quadratically with the model size. In practice, we are unable to run it with large model sizes, e.g., 128,000 centers for ImageNet data.

We summarize all empirical results in Figure 6 and demonstrate that our method achieves both linear memory complexity and linear time complexity (empirically verified) with respect to model size, offering the best of both worlds. For the ImageNet dataset, we trained all methods until convergence. While EigenPro 3 does not have the quadratic memory scaling problem, Figure 6 shows that even for a relatively small dataset like ImageNet with 1M data points, training a model size of 512,000 centers requires approximately 43 days on a single GPU to reach convergence (about 100 epochs). In contrast, our proposed model achieves convergence in approximately 3 hours, requiring only 15 epochs, with each epoch being significantly more computationally efficient than EigenPro 3 (see Table 2).

Faster Convergence with EigenPro 4. EigenPro 4 generally demonstrates the fastest convergence among all tested methods. In certain cases, such as ImageNet with 1.2 million model centers, EigenPro 4 converges in less than 10% of the epochs needed by other methods, while also delivering superior model performance. Figure 5 compares Eigen-

Pro 4 and EigenPro 3 across multiple training epochs, following the experimental setup established in Abedsoltan et al. (2023). Despite EigenPro 4’s linear time complexity per iteration (compared to EigenPro 3’s quadratic complexity), it demonstrates faster convergence with fewer epochs. This efficiency gain is particularly pronounced for larger model sizes, where EigenPro 4 maintains or exceeds EigenPro 3’s accuracy while requiring significantly fewer epochs. These results empirically validate that EigenPro 4’s algorithmic improvements translate to practical benefits: not only does each iteration run faster, but fewer iterations are needed to achieve optimal performance across diverse datasets. This empirically shows that our model has a linear time complexity with respect to the model size.

6 CONCLUSION

In this work, we introduced EigenPro 4, an advancement in training large kernel models that achieves linear time complexity per iteration and linear memory scaling with model size. By implementing a delayed projection strategy, we addressed the high computational overhead previously associated with frequent projections, achieving significant time and memory efficiency improvements over EigenPro 3 and Falkon. Our empirical results on diverse datasets highlight EigenPro 4 ability to match or exceed the performance of prior methods with vastly reduced computational resources. Specifically, the algorithm demonstrates both faster convergence and superior scalability, enabling training with model sizes and datasets that were previously infeasible due to memory and time constraints.

Furthermore, EigenPro 4 design opens up new possibilities for parallelization, as it is well-suited for multi-GPU and distributed architectures. Future work will explore these aspects, further expanding its potential in real-world applications requiring efficient, scalable kernel methods for massive data volumes.

Acknowledgements: We acknowledge support from the National Science Foundation (NSF) and the Simons Foundation for the Collaboration on the Theoretical Foundations of Deep Learning through awards DMS-2031883 and #814639, the TILOS institute (NSF CCF-2112665), and the Office of Naval Research (N8644-NV-ONR). This work used ACCESS (Advanced cyberinfrastructure coordination ecosystem: services & support) which is supported by NSF grants numbers #2138259, #2138286, #2138307, #2137603, and #2138296. Specifically, we used the resources from SDSC Expanse GPU compute nodes, and NCSA Delta system, via allocations TG-CIS220009. This work was done in part while AA was visiting the Simons Institute for the Theory of Computing. PP was supported by the DST INSPIRE Faculty Fellowship, and a Thakur Family Chair at C-MInDS, IIT Bombay.

REFERENCES

- Amirhesam Abedsoltan, Mikhail Belkin, and Parthe Pandit. Toward large kernel models. In *Proceedings of the 40th International Conference on Machine Learning, ICML’23*. JMLR.org, 2023.
- Amirhesam Abedsoltan, Mikhail Belkin, Parthe Pandit, and Luis Rademacher. On the nystrom approximation for preconditioning in kernel machines. *27th International Conference on Artificial Intelligence and Statistics (AISTATS)*, 2024.
- Mikhail Belkin, Siyuan Ma, and Soumik Mandal. To understand deep learning we need to understand kernel learning. In *International Conference on Machine Learning*, pages 541–549. PMLR, 2018.
- Mikhail Belkin, Daniel Hsu, Siyuan Ma, and Soumik Mandal. Reconciling modern machine-learning practice and the classical bias–variance trade-off. *Proceedings of the National Academy of Sciences*, 116(32):15849–15854, 2019.
- Raffaello Camoriano, Tomás Angles, Alessandro Rudi, and Lorenzo Rosasco. Nytro: When subsampling meets early stopping. In *Artificial Intelligence and Statistics*, pages 1403–1411. PMLR, 2016.
- Jia Deng, Wei Dong, Richard Socher, Li-Jia Li, Kai Li, and Li Fei-Fei. Imagenet: A large-scale hierarchical image database. In *2009 IEEE conference on computer vision and pattern recognition*, pages 248–255. Ieee, 2009.
- Jacob Gardner, Geoff Pleiss, Ruihan Wu, Kilian Weinberger, and Andrew Wilson. Product kernel interpolation for scalable gaussian processes. In *International Conference on Artificial Intelligence and Statistics*, pages 1407–1416. PMLR, 2018.
- Like Hui and Mikhail Belkin. Evaluation of neural architectures trained with square loss vs cross-entropy in classification tasks. In *International Conference on Learning Representations*, 2021. URL <https://openreview.net/forum?id=hsFN92eQEla>.
- Arthur Jacot, Franck Gabriel, and Clément Hongler. Neural tangent kernel: Convergence and generalization in neural networks. *Advances in neural information processing systems*, 31, 2018.
- Dan Jurafsky. *Speech & language processing*. Pearson Education India, 2000.
- Alex Krizhevsky, Geoffrey Hinton, et al. Learning multiple layers of features from tiny images. *CiteSeer*, 2009.
- Wen Li, Limin Wang, Wei Li, Eirikur Agustsson, and Luc Van Gool. Webvision database: Visual learning and understanding from web data. *arXiv preprint arXiv:1708.02862*, 2017.
- Siyuan Ma and Mikhail Belkin. Diving into the shallows: a computational perspective on large-scale shallow learning. *Advances in neural information processing systems*, 30, 2017.
- Siyuan Ma and Mikhail Belkin. Kernel machines that adapt to gpus for effective large batch training. *Proceedings of Machine Learning and Systems*, 1:360–373, 2019.
- Alexander G. de G. Matthews, Mark van der Wilk, Tom Nickson, Keisuke Fujii, Alexis Boukouvalas, Pablo León-Villagr a, Zoubin Ghahramani, and James Hensman. GPflow: A Gaussian process library using TensorFlow. *Journal of Machine Learning Research*, 18(40): 1–6, apr 2017. URL <http://jmlr.org/papers/v18/16-537.html>.
- Giacomo Meanti, Luigi Carratino, Lorenzo Rosasco, and Alessandro Rudi. Kernel methods through the roof: handling billions of points efficiently. *Advances in Neural Information Processing Systems*, 33:14410–14422, 2020.
- Preetum Nakkiran, Behnam Neyshabur, and Hanie Sedghi. The deep bootstrap framework: Good online learners are good offline generalizers. *International Conference on Learning Representations*, 2021.

- Vassil Panayotov, Guoguo Chen, Daniel Povey, and Sanjeev Khudanpur. Librispeech: an asr corpus based on public domain audio books. In *2015 IEEE international conference on acoustics, speech and signal processing (ICASSP)*, pages 5206–5210. IEEE, 2015.
- Pratik Rathore, Zachary Frangella, and Madeleine Udell. Have askotch: Fast methods for large-scale, memory-constrained kernel ridge regression. *arXiv preprint arXiv:2407.10070*, 2024.
- Alessandro Rudi, Luigi Carratino, and Lorenzo Rosasco. Falkon: An optimal large scale kernel method. *Advances in neural information processing systems*, 30, 2017.
- Shai Shalev-Shwartz, Yoram Singer, and Nathan Srebro. Pegasos: Primal estimated sub-gradient solver for svm. In *Proceedings of the 24th international conference on Machine learning*, pages 807–814, 2007.
- Michalis Titsias. Variational learning of inducing variables in sparse gaussian processes. In *Artificial intelligence and statistics*, pages 567–574. PMLR, 2009.
- J. Towns, T. Cockerill, M. Dahan, I. Foster, K. Gaither, A. Grimshaw, V. Hazlewood, S. Lathrop, D. Lifka, G. D. Peterson, R. Roskies, J. Scott, and N. Wilkins-Diehr. Xsede: Accelerating scientific discovery. *Computing in Science & Engineering*, 16(05):62–74, sep 2014. ISSN 1558-366X. doi: 10.1109/MCSE.2014.80.
- Shinji Watanabe, Takaaki Hori, Shigeki Karita, Tomoki Hayashi, Jiro Nishitoba, Yuya Unno, Nelson Enrique Yalta Soplín, Jahn Heymann, Matthew Wiesner, Nanxin Chen, Adithya Renduchintala, and Tsubasa Ochiai. ESP-net: End-to-end speech processing toolkit. In *Proceedings of Interspeech*, pages 2207–2211, 2018. doi: 10.21437/Interspeech.2018-1456. URL <http://dx.doi.org/10.21437/Interspeech.2018-1456>.
- Ross Wightman. Pytorch image models. <https://github.com/rwightman/pytorch-image-models>, 2019.
- Christopher Williams and Matthias Seeger. Using the nyström method to speed up kernel machines. *Advances in neural information processing systems*, 13, 2000.
- Andrew Wilson and Hannes Nickisch. Kernel interpolation for scalable structured gaussian processes (kiss-gp). In *International conference on machine learning*, pages 1775–1784. PMLR, 2015.
- Chiyuan Zhang, Samy Bengio, Moritz Hardt, Benjamin Recht, and Oriol Vinyals. Understanding deep learning (still) requires rethinking generalization. *Communications of the ACM*, 64(3):107–115, 2021.

A CONVERGENCE ANALYSIS

In this section, we derive EigenPro4.0-Exact (Algorithm 2), a precursor to EigenPro4.0. However, this version does not scale efficiently. In Section 4, we enhance its scalability by introducing stochastic approximations, resulting in EigenPro4.0 (Algorithm 1).

Recall that the derivatives of the loss function, as defined in equation 19, lie in the span of the training data, denoted as \mathcal{X} . However, these derivatives cannot directly update the model, which resides in the span of the model centers, \mathcal{Z} . To address this, we first fit the labels within the \mathcal{X} and then project the solution into the \mathcal{Z} . This process is repeated iteratively on the residual labels until convergence, as outlined in Algorithm 2.

Algorithm 2 EigenPro 4-Exact

Require: Data (X, \mathbf{y}) , centers Z

- 1: $\tilde{\mathbf{y}}_0 = \mathbf{y}$
 - 2: **for** $t = 1, 2, \dots$ **do**
 - 3: $\boldsymbol{\alpha}_t = K^{-1}(X, X)\tilde{\mathbf{y}}_t$
 - 4: $K(\cdot, Z)\boldsymbol{\beta}_t = \text{proj}_{\mathcal{Z}}(K(\cdot, X)\boldsymbol{\alpha}_t)$
 - 5: $\tilde{\mathbf{y}}_{t+1} = \mathbf{y} - K(X, Z)\boldsymbol{\beta}_t$
 - 6: **end for**
-

The following proposition provides the fixed point analysis for this algorithm.

Proposition 1. Consider any dataset X, \mathbf{y} and a choice of model centers Z , with a kernel function $K : \mathbb{R}^d \times \mathbb{R}^d \rightarrow \mathbb{R}$. Assume that $K(X, X)$ and $K(Z, X)$ are full Rank. Then, Algorithm 2 converges to the following solution:

$$\hat{f} = K(\cdot, Z) \left(K(Z, X)K^{-1}(X, X)K(X, Z) \right)^{-1} K(Z, X)K^{-1}(X, X)\mathbf{y}. \quad (28)$$

Furthermore, if $\mathbf{y} = K(X, Z)\boldsymbol{\beta}^* + \boldsymbol{\xi}$, where $\boldsymbol{\xi}$ is a vector of independent centered random noise with $\mathbb{E}[\xi_i^2] = \sigma^2$, then

$$\lim_{t \rightarrow \infty} \mathbb{E}[\boldsymbol{\beta}_t] = \boldsymbol{\beta}^*, \quad \lim_{t \rightarrow \infty} \frac{\mathbb{E}[\|\boldsymbol{\beta}_t - \boldsymbol{\beta}^*\|^2]}{\sigma^2} = \text{tr} \left(\left(K(Z, X)K^{-1}(X, X)K(X, Z) \right)^{-2} K(Z, X)K^{-2}(X, X)K(X, Z) \right).$$

This algorithm has a major drawback, as solving the problem in the \mathcal{X} is inherently more challenging. However, in the next section, we demonstrate how to effectively scale this approach.

Proposition 2. Consider any dataset X, \mathbf{y} and a choice of model centers Z , with a kernel function $K : \mathbb{R}^d \times \mathbb{R}^d \rightarrow \mathbb{R}$. Assume that $K(X, X)$ and $K(Z, X)$ are full Rank. Then, Algorithm 2 converges to the following solution:

$$\hat{f} = K(\cdot, Z)K^+(Z, X)\mathbf{y}. \quad (29)$$

Furthermore, if $\mathbf{y} = K(X, Z)\boldsymbol{\beta}^* + \boldsymbol{\xi}$, where $\boldsymbol{\xi}$ is a vector of independent centered random noise with $\mathbb{E}[\xi_i^2] = \sigma^2$, then

$$\lim_{t \rightarrow \infty} \mathbb{E}[\boldsymbol{\beta}_t] = \boldsymbol{\beta}^*, \quad \lim_{t \rightarrow \infty} \frac{\mathbb{E}[\|\boldsymbol{\beta}_t - \boldsymbol{\beta}^*\|^2]}{\sigma^2} = \text{tr} \left(\left(K(Z, X)K^{-1}(X, X)K(X, Z) \right)^{-2} K(Z, X)K^{-2}(X, X)K(X, Z) \right).$$

Proof. We begin by expressing Algorithm 2 recursively and substituting $\text{proj}_{\mathcal{Z}}$ with the expression in equation 20. Recall that $f_t = K(\cdot, Z)\boldsymbol{\beta}_t$ with base case $\boldsymbol{\beta}_0 = 0$. The update rule for $\boldsymbol{\beta}_t$ is given by:

$$\boldsymbol{\beta}_t = K^{-1}(Z, Z)K(Z, X)K^{-1}(X, X)(\mathbf{y} - K(X, Z)\boldsymbol{\beta}_{t-1}) + \boldsymbol{\beta}_{t-1}. \quad (30)$$

Let us define the matrices:

$$B := K^{-1}(Z, Z)K(Z, X)K^{-1}(X, X), \quad C := BK(X, Z) - I,$$

which allows us to rewrite the recursion more succinctly:

$$\begin{aligned} \beta_t &= B(\mathbf{y} - K(X, Z)\beta_{t-1}) + \beta_{t-1} \\ &= B\mathbf{y} - C\beta_{t-1} = B\mathbf{y} - CB\mathbf{y} + C^2\beta_{t-2} \\ &\vdots \\ &= \left(\sum_{i=0}^{t-1} (-1)^i C^i \right) B\mathbf{y}. \end{aligned} \tag{31}$$

As the number of iterations tends to infinity, we can define the infinite series sum:

$$S := \sum_{i=0}^{\infty} (-1)^i C^i.$$

Observe that:

$$S + CS = I.$$

Substituting the definition $C = BK(X, Z) - I$ and $B = K^{-1}(Z, Z)K(Z, X)K^{-1}(X, X)$, we have:

$$K^{-1}(Z, Z)K(Z, X)K^{-1}(X, X)K(X, Z)S = I.$$

Thus, this simplifies to:

$$S = (K(Z, X)K^{-1}(X, X)K(X, Z))^{-1} K(Z, Z).$$

Therefore, the final solution converges to:

$$\hat{f} = K(\cdot, Z) (K(Z, X)K^{-1}(X, X)K(X, Z))^{-1} K(Z, X)K^{-1}(X, X)\mathbf{y}. \tag{32}$$

Substituting $\mathbf{y} = K(X, Z)\beta^* + \boldsymbol{\xi}$ readily completes the second claim. □

B COMPUTATIONAL COMPLEXITY COMPARISON

We assume that EigenPro4 is processing T batches of data at once before running the post-processing step of projection. Here we show we calculated the optimal value of T .

Cost for processing t^{th} batch of data. For a some $k \in \mathbb{N}$, let $kT < t \leq (k+1)T$. See Table 3.

Cost of processing T batches of data before post-processing The total cost for processing T batches $t = kT + 1$ to $t = (k+1)T$ before the projection is the sum of the above

$$T(2mp + 2ms + 2sq + pq) + m^2 \sum_{t=kT+1}^{(k+1)T} (t - kT - 1) = T(2mp + 2ms + 2sq + pq) + m^2 \frac{T(T-1)}{2} \tag{33}$$

line	computation	flops
10	$K(X_m, Z)\alpha - \mathbf{y}_t$	mp
11	$K(X_m, Z_{\text{tmp}})\alpha_{\text{tmp}}$	$m^2(t - kT - 1)$
12	$K(X_m, X_s)\alpha_s$	ms
15,17	$\mathbf{h}_1 := \mathbf{F}^\top K(X_s, X_m)\mathbf{g}_m \in \mathbb{R}^q$	$ms + sq$
15	$\mathbf{F}\mathbf{h}_1$	sq
17	$K(Z, X_m)\mathbf{g}_m$	mp
17	$\mathbf{M}\mathbf{h}_1$	pq

Table 3: Computational cost analysis of Algorithm 1 for processing batch t for $kT < t \leq (k+1)T$ for some $k \in \mathbb{N}$. The cost of processing batch t without the post-processing adds up to $2mp + 2ms + 2sq + pq + m^2(t - kT - 1)$ flops.

Average of processing T batches of data with post-processing Assuming the post processing involves T_{ep2} epochs of EigenPro 2, the average cost of processing T batches is

$$\frac{T(2mp + 2ms + 2sq + pq) + m^2 \frac{T(T-1)}{2} + p^2 T_{\text{ep2}}}{T} \quad (34)$$

A simple calculation shows that

$$T^* = \frac{p}{m} \sqrt{2T_{\text{ep2}}} \quad (35)$$

minimizes the average time above. The average cost of processing a batch is thus

$$2mp(1 + \sqrt{2T_{\text{ep2}}}) + 2ms + 2sq + pq \quad (36)$$

Algorithm	setup	FLOPS per batch*	Memory
EigenPro 4.0	$O(s^2q)$	$2mp(1 + \sqrt{2T_{\text{ep2}}}) + 2ms + 2sq + pq$	$s^2 + p(1 + \sqrt{2T_{\text{ep2}}})$
EigenPro 3.0	$O(s^2q)$	$2mp + p^2 T_{\text{ep2}} + 2ms + 2sq + pq$	$s^2 + p$
Falkon	$O(p^3)$	$2mp$	p^2

Table 4: **Comparing complexity of algorithms.** Number of training samples n , number of model centers p , batch size m , Nyström sub-sample size s , preconditioner level q . Here we assumed only a constant number of epochs of EigenPro 2.0 is needed for large scale experiments. Cost of kernel evaluations and number of classes are assumed to be $O(1)$, also it is reasonable to assume $p \gg s \gg q$.

* FLOPS per iteration reported are amortized over multiple batches processed.

C EXPERIMENTS RESULTS

C.1 Computational resources used

This work used the Extreme Science and Engineering Discovery Environment (XSEDE) (Townes et al., 2014). We used machines with NVIDIA-V100, NVIDIA-A100 and NVIDIA-A40 GPUs, with a V-RAM up to 1.3 T, and 8x cores of Intel(R) Xeon(R) Gold 6248 CPU @ 2.50GHz with a RAM of 100 GB. Note that we had 1.3T of ram for just one experiment CIFAR5M*, for the rest of experiments we were constraint with 400G of ram.

C.2 Datasets

We perform experiments on these datasets: (1) CIFAR10, Krizhevsky et al. (2009), (2) CIFAR5M, Nakkiran et al. (2021), (3) ImageNet, (4) Webvision.Li et al. (2017), and (5) librispeech.

CIFAR5M. In our experiments, we utilized both raw and embedded features from the CIFAR5M data-set. The embedded features were extracted using a MobileNetv2 model pre-trained on the ImageNet data-set, obtained from *timm* library Wightman (2019). We indicate in our results when pre-trained features were used by adding an asterisk (*) to the corresponding entries.

ImageNet. In our experiments, we utilized embedded features from the ImageNet data-set. The embedded features were extracted using a MobileNetv2 model pre-trained on the ImageNet dataset, obtained from *timm* library [Wightman \(2019\)](#). We indicate in our results when pre-trained features were used by adding an asterisk (*) to the corresponding entries.

Webvision. In our experiments, we utilized embedded features from the Webvision data-set. The embedded features were extracted using a ResNet-18 model pre-trained on the ImageNet dataset, obtained from *timm* library [Wightman \(2019\)](#). Webvision data set contains 16M images in 5k classes. However, we only considered the first 2k classes.

Librispeech. Librispeech [Panayotov et al. \(2015\)](#) is a large-scale (1000 hours in total) corpus of 16 kHz English speech derived from audio books. We choose the subset train-clean-100 and train-clean-300 (5M samples) as our training data, test-clean as our test set. The features are got by passing through a well-trained acoustic model (a VGG+BLSTM architecture in [Hui and Belkin \(2021\)](#)) to align the length of audio and text. It is doing a 301-wise classification task where different class represents different uni-gram [Jurafsky \(2000\)](#). The implementation of extracting features is based on the ESPnet toolkit [Watanabe et al. \(2018\)](#).

C.3 Experiments details

Figure 1 This experiment used CIFAR5M* data set, where embedding has been generated using a pre-trained mobile-net network mentioned earlier. this is the only experiment that we had access to 1.3T of VRAM. We set the bandwidth to 5.0 and use 1k Nystrom samples with preconditioning level of size 100. We used float16 for this experiment.

Figure 3 This experiment has been run over Webvision data set with extracted embedding through Resnet18. the model size here is set to 100k number of centers. The bandwidth used is 5.0, 1k Nystrom samples with preconditioning level of size 100. We used float16 for this experiment.

Figure 5 We follow the setting in [Abedsoltan et al. \(2023\)](#). The bandwidth used here is 20 for Librispeech and Webvision and 16 for imagenet. Here again we used extracted feature of these datasets mentioned earlier. The precision used here is float32. with 10k Nystrom samples with preconditioning level of size 1000.

Figure 6 We used the same experiment setting in Figure 5.

Table 2 For all datasets here we used bandwidth of 5.0 with 1k Nystrom samples with preconditioning level of size 100. We used float16 for all dataset except for Librispeech where we used float32. Further, we note that `Falkon` latest library ran out of GPU memory for model sizes larger than 256000 number of centers that is the reason we could not run it for 256000. And as mentioned for model sizes 521000 and above the algorithm has inherent quadratic scaling with respect to model size and we ran out of VRAM. In the plot we refer to both of these memry issues as OOM.